Monostatic RCS Analysis of Electrically Large Structures using Integral Equations

Oscar Borries, Erik Jørgensen, Peter Meincke
TICRA
Copenhagen, Denmark
{ob,ej,pme}@ticra.com

***Abstract*—The monostatic radar cross section (RCS) is an important design parameter for many applications but accurate RCS prediction of an electrically large structure continues to be a challenging task. High accuracy demands and a complicated geometry often mean that asymptotic methods are not applicable, while a full-wave method has traditionally required very large computational resources. In the present paper, we avoid the $\mathcal{O}(f^6)$ computational time scaling of the Method of Moments by applying the Multi-Level Fast Multipole Method (MLFMM). A range of modifications to the traditional way of applying MLFMM to monostatic RCS are implemented in order to achieve strong computational performance even on modest hardware.**

***Index Terms*—RCS, MLFMM, Integral Equations.**

I. Introduction

In many modern engineering tasks, the computation of the monostatic Radar Cross Section (RCS) is a critical part of the design process. The need for high accuracy often necessitates the use of full-wave methods to take into account effects that asymptotic methods cannot include accurately. Unfortunately, full-wave methods have traditionally been too computationally demanding for use in monostatic RCS computation of large structures. For full-wave methods based on an integral equation formulation, such as Method of Moments (MoM), the computation time scales as $\mathcal{O}(f^6)$, where f is the frequency. For the current state-of-the-art RCS prediction tools, this poor frequency scaling have resulted in algorithms [1], [2] that either relax the accuracy requirements by using asymptotic methods or, for implementations using full-wave methods, require extreme runtimes even on very advanced and expensive computing platforms [3], [4].

Acceleration algorithms such as the Multi-Level Fast Multipole Method (MLFMM) reduce the computational scaling of MoM to $O(C(f,P)f^2 \log f)$, where $C(f,P)$ is the number of iterations required for convergence of an iterative solver, and P is the number of incidence angles. Despite this significant reduction in computing resources, most state-of-the-art full-wave RCS solvers avoid the use of MLFMM and instead prefer MoM for a number of reasons. First, many low-order MLFMM codes are optimized for structures that are much larger than those feasible for monostatic RCS computations. Second, the number of iterations $C(f,P)$ can be very large because the number of incidence angles can be very large, so a direct solution is preferred. Third, most research for full-wave RCS has focused on advanced computing platforms, such as computing clusters, Graphics Processing Units (GPUs), or out-of-core implementations on Solid State Disks (SSDs), most of which are much harder to utilize for MLFMM than for MoM.

In this paper, we describe a range of developments towards an efficient algorithm for large-scale full-wave monostatic RCS, in particular for structures that are too large to handle with MoM. The algorithm includes a discretization based on higher-order basis functions and curved quadrilaterals, an MLFMM implementation focused on keeping memory requirements low, and a number of techniques that reduces the total number of matrix-vector products needed for computing the RCS for many incidence angles.

II. Monostatic Radar Cross Section

The Radar Cross Section $\sigma(\theta_u, \phi_u)$ of a structure in the direction (θ_u, ϕ_u) is generally defined as [5, p. 64]

$$\sigma(\theta_u, \phi_u) = \lim_{r\to\infty} 4\pi r^2 \frac{|\boldsymbol{E}^S(\theta_u, \phi_u)|^2}{|\boldsymbol{E}^I(\theta_i, \phi_i)|^2}, \tag{1}$$

where $\boldsymbol{E}^I(\theta_i, \phi_i) = \boldsymbol{E}_0 e^{-jk\hat{\boldsymbol{k}}\cdot\overline{r}}$ is the incident electric field due to a plane wave with constant amplitude vector $\boldsymbol{E}_0$ and propagation vector $\hat{\boldsymbol{k}} = -(\sin\theta_i \cos\phi_i \hat{\boldsymbol{x}} + \sin\theta_i \sin\phi_i \hat{\boldsymbol{y}} + \cos\theta_i \hat{\boldsymbol{z}})$, k is the free-space wavenumber, and $\boldsymbol{E}^S(\theta_u, \phi_u)$ is the scattered far-field in direction θ_u, ϕ_u. Note from (1) that the RCS can be considered a function defined on the unit sphere. The far-field RCS in (1) is typically the object of main practical interest, but it is possible to define and compute near-field RCS as well which has little impact on the solution process. Considering monostatic ($\theta_i = \theta_u, \phi_i = \phi_u$) rather than bistatic RCS significantly complicates the problem, since the current distribution on the target must be computed for each incidence direction.

The definition (1) does not take into account the polarization of the incident and scattered fields. We can define the $\hat{\boldsymbol{\psi}}$-polarized RCS for a $\hat{\boldsymbol{\nu}}$-polarized incident field as follows:

$$\sigma(\theta_u, \phi_u)_{\psi\nu} = \lim_{r\to\infty} 4\pi r^2 \frac{|\boldsymbol{E}^S(\theta_u, \phi_u)\cdot\hat{\boldsymbol{\psi}}|^2}{|\boldsymbol{E}^I_{\hat{\boldsymbol{\nu}}}(\theta_i, \phi_i)|^2}, \tag{2}$$

where we define $\boldsymbol{E}^I_{\hat{\boldsymbol{\nu}}}(\theta_i, \phi_i)$ as the electric field due to a $\boldsymbol{\nu}$-polarized plane-wave impinging from the direction (θ_i, ϕ_i). Generally, one chooses the polarization vectors as the spherical unit vectors, i.e. $\hat{\boldsymbol{\psi}}, \hat{\boldsymbol{\nu}} = \hat{\boldsymbol{\theta}}, \hat{\boldsymbol{\phi}}$.

III. Integral Equations

We consider the integral equation for time-harmonic electromagnetic waves and a perfectly electrically conducting (PEC) scatterer $\mathcal{S}$. The integral equation can be expressed as a mixed potential Electric Field Integral Equation (EFIE). On closed parts of $\mathcal{S}$, the Combined Field Integral Equation (CFIE) is used to avoid internal resonances. Through the Galerkin approach, a matrix equation $\overline{\overline{Z}}\,\overline{I} = \overline{V}$ is obtained. For monostatic RCS with P incidence angles, the system contains $2P$ right-hand sides (RHSs) and can be written as

$$\overline{\overline{Z}}\,\overline{\overline{I}} = \overline{\overline{V}}, \tag{3}$$

where $\overline{\overline{Z}}$ has the size $N \times N$ and $\overline{\overline{I}}, \overline{\overline{V}}$ have the size $N \times 2P$.

The solution to (3) will yield the required surface current densities in $\overline{\overline{I}}$. The accuracy of $\overline{\overline{I}}$ and the efficiency of the solution of (3) depend on the discretization. This motivates our choice of discretization scheme which is inherited from GRASP's MLFMM solver, where both the current $\boldsymbol{J}_{\mathcal{S}}$ and the surface geometry $\mathcal{S}$ are discretized using a higher-order approach [6]. With such a higher-order discretization, rather than one based on lower-order functions such as RWG [7], the number of unknowns N required for obtaining a specific accuracy is significantly reduced, which is critical because solving (3) requires $\mathcal{O}(C(f,P)N^2)$ operations for an iterative solution or $\mathcal{O}(N^3 + PN^2)$ for a direct solution.

A. Multi-Level Fast Multipole Method

To avoid the N^2 and N^3 terms in the asymptotic scaling, the Multi-Level Fast Multipole Method (MLFMM) is a procedure for performing the operation $\overline{\overline{Z}}\,\overline{I}$ in $\mathcal{O}(N \log N)$ time and memory. Combining this with an iterative solver such as GMRES allows us to solve (3) in $\mathcal{O}(C(f,P)N \log N)$ operations. While the standard MLFMM for RWG basis functions is well studied, it is not straight-forward to adapt MLFMM to a higher-order discretization. However, within the last couple of years, an efficient HO MLFMM formulation has been presented [8] and applied to a range of problems [9–11], demonstrating significantly better performance than standard MLFMM while being very suitable for commodity consumer hardware.

IV. Using MLFMM for monostatic RCS

While using MLFMM rather than MoM clearly yields a large reduction in memory footprint, it is not immediately clear that there is a reduction in runtime, since we have not yet quantified the number of iterations $C(f,P)$. Indeed, comparing our implementation to MoM-based RCS solvers such as [3], we clearly see that while MoM implementations focus on minimizing the number of unknowns N, our MLFMM implementation should focus on minimizing the number of iterations $C(f,P)$. This is an important methodological distinction, because many methods for reducing the number of unknowns are not error-controllable. In contrast, minimizing the number of iterations leads to approximations that are easier to control because they constitute algebraic errors made in solving the discrete system of equations.

To quantify the number of iterations $C(f,P)$ if the angular range is ϕ_{int}, we first consider the dependence of P on f by considering the angular sampling density [12]

$$P = \frac{\phi_{\text{int}}}{\Delta\phi} = \frac{4f\rho_{\max}\phi_{\text{int}}}{c_0} \tag{4}$$

where c_0 is the speed of light and $\rho_{\max}$ is the maximum object radius in the observation plane. We note that P is the number of right-hand sides for each polarization of the incident plane wave, thus the total number of right-hand sides will be $2P$. Thus, we can express $C(f,P)$ as

$$C(f,P) = 2N_{\text{it}}P, \tag{5}$$

where N_{it} is the number of iterations required for the iterative solver to converge for each of the $2P$ right-hand sides.

A. Interpolation techniques

Several interpolation techniques exist for relaxing the sampling density (4), either by interpolating the monostatic RCS result or by considering the columns in the $\overline{\overline{I}}$ matrix as being functions of (θ, ϕ) and performing interpolation to retrieve the current from additional incidence directions. We note that the interpolation is performed on each polarization independently, and thus considers only the P right-hand sides associated with each polarization rather than the total $2P$ right-hand sides.

1) Interpolating the monostatic RCS: The monostatic RCS can be interpolated by the many well-studied methods for interpolation of functions on a sphere. This is particularly relevant because the user might need a larger number of incidence angles P_u than required by the sampling criterion (4). In that case, when $P_u > P$, it is computationally much more efficient to solve (3) with P right-hand sides and then use interpolation, rather than solving (3) with P_u right-hand sides. The actual interpolation method depends on the distribution of the observation points:

- For full spherical cuts, i.e. scenarios where either θ or ϕ go through a full period, interpolation techniques based on the Fast Fourier Transform allow very high accuracies even with sparse samplings.
- For full spheres, i.e. scenarios where the entire far-field sphere is required, a number of highly efficient techniques exist, see e.g. [13].
- For partial cuts or grids, i.e. scenarios where θ and/or ϕ go through a subsection of their period, one has to resort to the usual local interpolation techniques such as Lagrange or Spline interpolation.

2) Interpolating the Current: Rather than interpolating the RCS, one can interpolate the current density considering the excitation of each basis function to be a function of angular coordinates. A number of these methods exist [3], [14], [15], but a particularly popular method is the Minimum Residual Interpolation method [16]. This method uses the QR factorization of the matrix $\overline{\overline{Z}}\,\overline{\overline{I}}(:, 1:k:P)$ in a hierarchical manner to allow interpolation of the remaining columns of $\overline{\overline{I}}$.

B. Iterative Solver

When using MLFMM, an iterative solver is needed to solve the problem in Eq. (3). The most popular solver for MLFMM problems appears to be the GMRES [17], which in its basic formulation is a Krylov method based on a single right-hand side. Thus, aside from reusing starting guesses [18], a standard textbook RCS implementation does not exploit the fact that the P systems in (3) are related. To improve on this, we have implemented a Block-GMRES solver as discussed in [19]. Rather than minimizing the residual $\overline{R} = \overline{\overline{Z}}\,\overline{I} - \overline{V}$ over the Krylov space $\{\overline{R}, \overline{\overline{Z}}\,\overline{R}, \overline{\overline{Z}}^2\overline{R}, \ldots\}$, the Block-GMRES minimizes all P residuals $\overline{\overline{R}} = \overline{\overline{Z}}\,\overline{\overline{I}} - \overline{\overline{V}}$ simultaneously over the Krylov space $\{\overline{\overline{R}}, \overline{\overline{Z}}\,\overline{\overline{R}}, \overline{\overline{Z}}^2\overline{\overline{R}}, \ldots\}$. A Block-Krylov solver provides a lower number of matrix-vector products than the $N_{\text{it}}P$ estimate given in (5) by utilizing information from all the P right-hand sides simultaneously. We stress that our implementation employs *deflation*. Deflation for Krylov solvers involves reducing the dimension of the Krylov subspace from P columns to P_d columns by applying a rank-revealing decomposition to the orthogonalized residual space.

V. Results

In this section, we compute the monostatic RCS from 4 structures using the scheme outlined above, which has been integrated with an MLFMM solver derived from GRASP. As in the previous section, we use the symbol P_u to denote the number of RHS requested by the user to stress that the number of right-hand sides P actually involved in the computation can be substantially lower than that. Further, the number of RHS actually involved in the iterative solver is P_d. We note that while some papers such as [3] only consider monostatic RCS from scatterers with symmetry planes, which can be exploited to yield better performance, none of the following results exploit any kind of symmetry.

A. Sphere

We begin with a simple canonical test-case, a PEC sphere of radius $r = 1\,\text{m}$. We use a Late 2013 MacBook Pro laptop with a 2.6 GHz i7 processor. Considering the frequency $f = 2.25\,\text{GHz}$, the sphere has an electrical radius of 7.51λ and is discretized with $N = 19200$ 5th-order basis-functions. CFIE is applied. From (4) we find that $P = 189$ right-hand sides for each polarization are necessary to characterize the monostatic RCS in a full spherical cut, although we note that only a single excitation for each polarization would be required for this special scatterer, due to its special symmetry properties.

First, we compute the result with MoM, which requires about 3 minutes of computation time and about 2.7 GB of memory. Most of the time is spent computing and factorizing the $\overline{\overline{Z}}$ matrix, while applying the forward/backward solver needed to find $\overline{\overline{I}}$ takes a few seconds. We note that a RWG-based MoM solution would require about 53 GB. For the MLFMM solution, about 0.5 GB of memory is required, and the computation takes 8 minutes, with deflation yielding $P_d = 105$ for each polarization. Thus, while the small electrical size of the problem leads to MLFMM being slower than MoM, the memory benefit from MLFMM is significant.

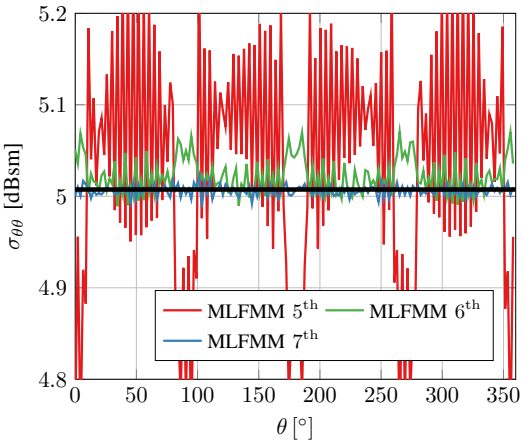

Fig. 1. Co-polar monostatic RCS for the sphere discussed in Section V-A for a full spherical cut for $\phi = 0$. The solid black line indicates the exact solution. Note the narrow range of the y-axis.

TABLE I
Simulation details for the experiments in Section V-A.

Basis fun. order	N	Memory [GB]	Time [min]	RMS
5th	19200	0.5	8	3.1%
6th	30000	0.9	14	0.4%
7th	43200	1.5	27	0.1%

The spherical target allows us to quantify the accuracy of the simulation by comparing with the analytical solution for the monostatic RCS from a PEC sphere [20, (6.47)], which yields $\sigma_{\theta\theta} = \sigma_{\phi\phi} = 3.168\,\text{m}^2 = 5.007\,\text{dBsm}$. The simulation results are shown in Figure 1 for the co-polar component and key performance data are summarized in Table I. In particular, we note from Figure 1 that the results converge nicely to the analytical value. We stress that the plot has a very narrow range of values on the y-axis, spanning an interval of only 0.4 dB, far within the required accuracy for most RCS applications. Further, the results in Figure 1 show the benefits of increasing the discretization accuracy, while Table I shows the associated computational costs. The distinct error patterns for the 5th and 6th order discretizations are due to mesh effects, which are only visible for the present case because the sphere is electrically small.

B. Helicopter

As a more realistic example, we now consider the simulation of a CAD model of a PEC helicopter shown in Figure 2. To challenge the implementation more thoroughly, the frequency is increased to 8 GHz in order to get an electrically much larger structure. Thus, we move from our laptop to a workstation, a Dual Intel Xeon E5-2690 2.9 GHz computer with 16 cores, to perform the simulation. With the longest dimension of the helicopter being about 7 meter for a full spherical cut in θ, (4) suggests that about $P = 2012$ incident directions are needed for each polarization, for a total of 4024 right-hand sides to be solved. We note that the structure does not have

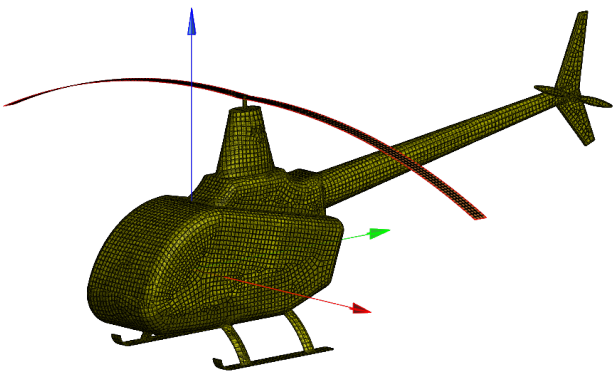

Fig. 2. Mesh of helicopter at 8 GHz. The green see-through regions are solved using the CFIE. The red, green, blue axis indicate $\hat{\boldsymbol{x}}, \hat{\boldsymbol{y}}, \hat{\boldsymbol{z}}$ unit vectors, respectively.

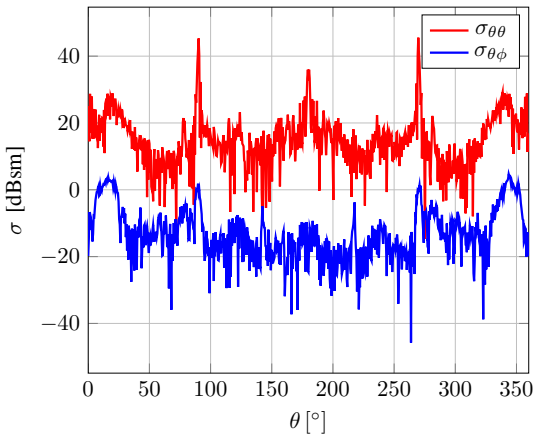

Fig. 3. Monostatic RCS for the helicopter discussed in Section V-B for a full spherical cut for $\phi = 0$.

any symmetry planes due to the tail rotor. Further, aside from the main rotor which is modelled as an infinitely thin curved plate and thus solved using EFIE, the body of the helicopter constitutes a closed structure where CFIE is applied. The mesh has patches of varying sidelengths, between $0.026\lambda - 1.78\lambda$, which are populated with basis functions up to 7th order depending on the size of the patch. The total number of basis functions is $N = 332879$, and thus a direct MoM solution using higher-order basis functions and the EFIE, similar to that applied in [3], would require 413 GB of storage. With our implementation, the maximum amount of memory used is about 20 GB, with another 25 GB of disk space used for storage of some components in the GMRES solver. The computation requires about 11 hours of computation time, with deflation yielding $P_d = 686$.

C. NASA Almond

The NASA Almond is a classic RCS benchmark, measured and described in [21] as a simple mathematical model, that none-the-less provides some challenges for monostatic RCS computations and measurements. We initially consider the target at 7 GHz, and compare our solution to the results from the original paper [21] as well as results from two popular

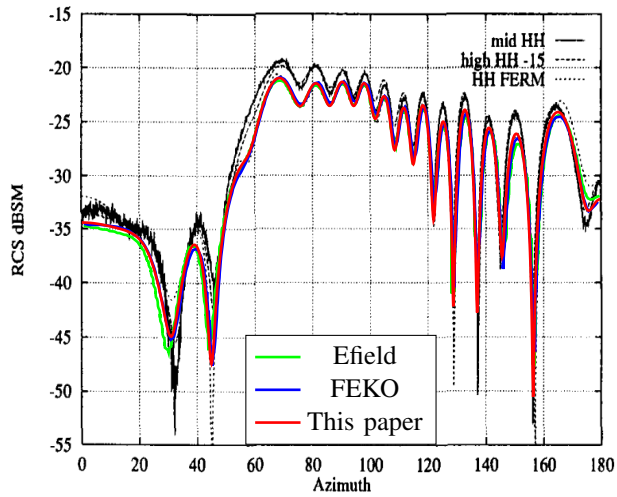

Fig. 4. RCS of the NASA Almond at 7 GHz. Comparison of 4 independent full-wave solutions and two sets of measurements.

TABLE II
SIMULATION DETAILS FOR THE EXPERIMENTS IN SECTION V-C. THE () NUMBERS INDICATE GB OF HARD-DISK USED.

Code	f [GHz]	N	Time [min]	Memory [GB]	Platform (Table III)
[24]	21	99915	61	3	Xeon
[24]	75	1043577	4369	113	Xeon
[25]	75	110000	438	194	HPC
[25]	150	370000	1140	2294	SSC
This paper	75	82494	110	7 (+3)	Laptop
This paper	150	302346	1053	12 (+17)	Laptop

TABLE III
DETAILS ON COMPUTING PLATFORMS FROM TABLE II.

Xeon	4 Xeon X5482 machine. Code implemented in Matlab.
HPC	6 node cluster, 2 Xeon E5620 on each node.
SSC	Shanghai Supercomputer Center 2011. 35 nodes, 16 cores on each node.
Laptop	2013 MacBook Pro i7 2.6 GHz.

software vendors, Efield [22] and FEKO [23]. This comparison is shown in Figure 4, along with the two sets of measurements from the original paper [21] and the MoM code from that paper (HH Ferm). Note that all four computational codes give nearly identical results, while the measurements deviate somewhat. Next, table II indicates the performance of our code compared with results found in the literature for the frequencies 21 GHz, 75 GHz, and 150 GHz. We stress that these results have been achieved on different computing platforms, as indicated by the right-most column in Table II which refers to Table III. While the tables offer several interesting conclusions, the main result is that MLFMM provides a very strong frequency scaling, allowing us to solve very large problems much more efficiently than other codes, even when running on a simple laptop.

D. Reentry vehicle

As a final example, we consider the shape described in [26], where a reentry vehicle is analyzed using the RCS module of the Lucernhammer software. The circular symmetric structure

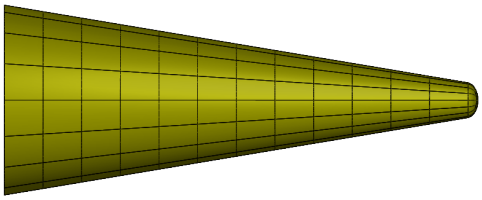

Fig. 5. Mesh of the PEC reentry vehicle. The structure is a body of revolution, with maximum diameter $0.4\,\mathrm{m}$ and a length of $1\,\mathrm{m}$.

TABLE IV
SIMULATION DETAILS FOR THE EXPERIMENTS IN SECTION V-D.

Code	f	N	Time [min]	Memory [GB]
[26]	$5\,\mathrm{GHz}$	155076	42	N/A
[26]	$9.5\,\mathrm{GHz}$	557436	828	N/A
Our - MoM	$5\,\mathrm{GHz}$	7340	0.5	0.45
Our - MLFMM	$5\,\mathrm{GHz}$	7340	2	0.25
Our - MoM	$9.5\,\mathrm{GHz}$	25312	6	4.82
Our - MLFMM	$9.5\,\mathrm{GHz}$	25312	11	0.81

is shown in Figure 5. The results in [26] were obtained by considering the structure at $f = 5\,\mathrm{GHz}$ and $f = 9.5\,\mathrm{GHz}$ using their RWG-based MoM code accelerated with the Adaptive Cross Approximation, running on a Intel Xeon W5580 workstation with 8 cores and 128 GB RAM. We run the case at the same frequencies, but restrict ourselves to using the MacBook Pro 2013 laptop discussed in Section V-A.

The important performance metrics are shown in Table IV. The benefits of our higher-order discretization, which also yields a very good mesh on this structure, is clear when compared with an RWG solver: A reduced number of unknowns leads to a much lower computation time (and presumably also memory, although memory counts are not available from [26]).

VI. CONCLUSION

It was shown that using MLFMM rather than MoM yields a faster and much less memory-intensive solution to the full-wave simulation of the monostatic RCS from a structure — indeed, the low asymptotic scaling of MLFMM allows electrically much larger problems to be solved even on modest computing hardware. Further, a range of efforts were described that significantly reduces the computational requirements while allowing strong error control, such as the use of higher-order basis functions, interpolation techniques, and an efficient iterative solver.

An early-stage implementation of these techniques was shown to provide high accuracy and strong performance on four examples, including a helicopter, the Nasa Almond, and a reentry vehicle, the latter of which allowed an independent illustration of the strengths of our higher-order discretization when compared to a commercial product based on the widely used RWG discretization.

REFERENCES

[1] Y. An, D. Wang, and R. Chen, "Improved multilevel physical optics algorithm for fast computation of monostatic radar cross section," *IET Microwaves, Antennas & Propagation*, vol. 8, pp. 93–98, Jan. 2014.

[2] K. Divyabramham and R. Vulapalli. RCS Predictions for Electrically Large Complex Structures. [Online]. Available: https://goo.gl/81QH5X

[3] M. S. Pavlovic, M. S. Tasic, B. L. Mrdakovic, and B. M. Kolundžija, "WIPL-D: Monostatic RCS Analysis of Fighter aircrafts," in *EuCAP 2016*. IEEE, Nov. 2016.

[4] G. Cakir, M. Cakir, and L. Sevgi, "Radar Cross Section (RCS) Modeling and Simulation, Part 2: A Novel FDTD-Based RCS Prediction Virtual Tool for the Resonance Regime," *IEEE Antennas and Propagation Magazine*, vol. 50, no. 2, pp. 81–94, Apr. 2008.

[5] E. F. Knott, J. Shaeffer, and M. Tuley, *Radar Cross Section*, 2nd ed. SciTech Publishing, Aug. 2004.

[6] E. Jørgensen, J. Volakis, P. Meincke, and O. Breinbjerg, "Higher Order Hierarchical Legendre Basis Functions for Electromagnetic Modeling," *IEEE Trans. Antennas Propag.*, vol. 52, pp. 2985–2995, Nov. 2004.

[7] S. M. Rao, D. R. Wilton, and A. W. Glisson, "Electromagnetic Scattering by Surfaces of Arbitrary Shape," *IEEE Trans. Antennas Propag.*, vol. 30, no. 3, pp. 409–418, May 1982.

[8] O. Borries, P. Meincke, E. Jørgensen, and P. C. Hansen, "Multi-level Fast Multipole Method for Higher-Order Discretizations," *IEEE Trans. Antennas Propag.*, vol. 62, no. 9, Sep. 2014.

[9] O. Borries, P. Meincke, E. Jørgensen, S. B. Sørensen, and P. C. Hansen, "Improved Multilevel Fast Multipole Method for Higher-Order Discretizations," in *EuCAP 2014*, 2014, pp. 3610–3614.

[10] E. Jørgensen, O. Borries, P. Meincke, and N. Vesterdal, "Fast Full-Wave Analysis of Challenging Reflector Antenna Problems," in *2015 IEEE Antennas and Propagation Society Int. Symp.*, 2015, pp. 1–2.

[11] O. Borries, E. Jørgensen, P. Meincke, and H.-H. Viskum, "Full-wave Optimization of Large Compact Antenna Test Ranges," in *EuCAP 2016*, Jan. 2016.

[12] H. Buddendick and T. F. Eibert, "Acceleration of Ray-Based Radar Cross Section Predictions Using Monostatic-Bistatic Equivalence," *IEEE Trans. Antennas Propag.*, vol. 58, no. 2, pp. 531–539, Jan. 2010.

[13] O. M. Bucci, C. Gennarelli, and C. Savarese, "Optimal Interpolation of Radiated Fields Over a Sphere," *IEEE Trans. Antennas Propag.*, vol. 39, no. 11, pp. 1633–1643, Nov. 1991.

[14] Z. W. Liu, R.-S. Chen, and J. Q. Chen, "Adaptive sampling cubic-spline interpolation method for efficient calculation of monostatic RCS," *Microw. Opt. Technol. Lett.*, vol. 50, no. 3, pp. 751–755, Mar. 2008.

[15] Z.-Q. Lu and X. An, "Fast monostatic radar cross-section computation for perfectly electric conducting targets using low-rank compression and adaptive integral method," *IET Microwaves, Antennas & Propagation*, vol. 8, no. 1, pp. 46–51, Jan. 2014.

[16] P. Lötstedt and M. Nilsson, "A Minimal Residual Interpolation Method for Linear Equations with Multiple Right-Hand Sides," *SIAM Journal on Scientific Computing*, vol. 25, no. 6, pp. 2126–2144, Jan. 2004.

[17] Y. Saad and M. H. Schultz, "GMRES: A Generalized Minimal Residual Algorithm for Solving Nonsymmetric Linear Systems," *SIAM J. Sci. Comput.*, vol. 7, no. 3, pp. 856–869, Jun. 1986.

[18] J. M. Song, C.-C. Lu, and W. C. Chew, "Multilevel Fast Multipole Algorithm for Electromagnetic Scattering by Large Complex Objects," *IEEE Trans. Antennas Propag.*, vol. 45, pp. 1488–1493, Oct. 1997.

[19] M. H. Gutknecht, "Block Krylov space methods for linear systems with multiple right-hand sides: an introduction," *Seminar for Applied Mathematics*, 2006.

[20] D. B. Davidson, *Computational Electromagnetics for RF and Microwave Engineering*, 2nd ed., Cambridge University Press, Jul. 2010.

[21] A. C. Woo, H. T. G. Wang, M. J. Schuh, and M. L. Sanders, "Benchmark Radar Targets for the Validation of Computational Electromagnetics Programs," *IEEE Antennas Propag. Mag.*, vol. 35, no. 1, pp. 84–89, Feb. 1993.

[22] Efield. Solutions NASA Almond RCS. [Online]. Available: https://goo.gl/njpwYI

[23] FEKO. RCS Measurement and Simulation of Generic Simple Shapes. [Online]. Available: https://goo.gl/fguLeW

[24] A. Heldring, J. M. Tamayo, E. Ubeda, and J. M. Rius, "Accelerated Direct Solution of the Method-of-Moments Linear System," *Proceedings of the IEEE*, vol. 101, no. 2, pp. 364–371, Feb. 2013.

[25] D. Garcia-Donoro, I. Martinez-Fernandez, L. E. García-Castillo, Y. Zhang, and T. K. Sarkar, "RCS Computation using a Parallel in-core and out-of-core Direct Solver," *PIERS*, vol. 118, pp. 505–525, 2011.

[26] W. Gibson. (2015, May) Adaptive Cross Approximation Solver in the Serenity Radar Cross Section Prediction Code. [Online]. Available: goo.gl/qBY0tt